J Mater Sci (2015) 50:1958–1964
DOI 10.1007/s10853-014-8760-8

Synthesis and characterization of $Sm(OH)_3$ and Sm_2O_3 nanoroll sticks

Jun-Gill Kang · Bong-Ki Min · Youngku Sohn

Received: 13 July 2014 / Accepted: 2 December 2014 / Published online: 9 December 2014

Abstract Hexagonal phase $Sm(OH)_3$ nanoroll sticks were first synthesized by hydrothermal method, and cubic phase Sm_2O_3 nanoroll sticks were obtained by post-annealing treatment at 450 °C. The growth of Sm_2O_3 nanoroll sticks was found to be [40-4] direction. Their characteristics were examined by scanning electron microscopy, transmission electron microscopy, X-ray diffraction crystallography, Raman, FT-IR, UV–Vis–NIR absorption, and temperature-programmed reduction experiment.

Introduction

Samarium oxide (Sm_2O_3) is a high-k dielectric material and has extensively been studied for its potential application to alternative gate dielectric in complementary metal–oxide–semiconductors (CMOS) and resistance random access memories (RRAM) [1–4]. Wang et al. used high-k Sm_2O_3 thin film as a pH-sensing layer [5]. Application to catalyst has also been of interest [6–10]. Elkins et al. demonstrated that Sm_2O_3 could be a promising catalyst for the oxidative coupling of methane [8]. Wang et al. reported a potential application to photocatalytic dye degradation [9, 10]. Many effects have been devoted to synthesize diverse morphologies of Sm_2O_3. $Sm(OH)_3$ has also been prepared since Sm_2O_3 could be obtained by a post-thermal dehydration [11, 12]. Facial solution-based synthetic methods include hydrothermal [13–15], precipitation [11, 16], sol–gel [18], and template [19] methods. Many different morphologies have been synthesized and reported, including nanorods [11, 15–17, 20], nanodisks [18], nanowires [21, 22], submicrospindles [23], nanoparticles [24], and nanoplates [20, 21]. Yu et al. synthesized single unit cell size (1.1 nm thick and 2.2 nm wide) Sm_2O_3 nanowires and nanoplates by thermal decomposition of Sm(III) acetate in the presence of oleylamine and a long-chain carboxylic acid under Ar atmosphere [21]. Panda et al. used the same chemicals but applied microwave to synthesize Sm_2O_3 nanorods [20]. Nejad et al. synthesized Sm_2O_3 nanoparticles (50–80 nm) in supercritical water condition by a hydrothermal method and reported BET surface areas of 20–32 m^2/g for the synthesized nanoparticles [14]. Sm_2O_3 fibers were prepared by thermal calcination of samarium citrate-PVA composite nanofibers, which were prepared by an electrospinning technique [25]. Precipitation method has also widely been employed to synthesize nanorods [11, 12]. Zhang et al. reported Sm_2O_3 mesoporous structures by a surfactant-mediated PMMA-template assisted synthesis and a post-thermal treatment [19].

In the present study, we first prepared $Sm(OH)_3$ and Sm_2O_3 nanoroll (rolled into nanotubes) sticks, which were then characterized using various experimental techniques. The morphology could be controlled by an amount of ammonia and a reaction temperature. Because new morphology generally exhibits different physicochemical properties and application performances [26] the newly found nanoroll stick morphology provides new insight for developing $Sm(OH)_3$ and Sm_2O_3 nanostructures for

J.-G. Kang
Department of Chemistry, Chungnam National University, Daejeon 305-764, South Korea

B.-K. Min
Centre for Research Facility, Yeungnam University, Gyeongsan, Gyeongbuk 712-749, South Korea

Y. Sohn (✉)
Department of Chemistry, Yeungnam University, Gyeongsan, Gyeongbuk 712-749, South Korea
e-mail: youngkusohn@ynu.ac.kr

various applications including high-k materials, catalysts, and sensors.

Experimental section

For the synthesis of $Sm(OH)_3$ nanoroll sticks, we prepared 25 mL of ~0.04 M Sm(III) sulfate octahydrate (Sigma-Aldrich, 99.9 %) solution and added 2.0 mL of ammonia solution (~30 %) drop-wise to obtain precipitates. The solution was then transferred to a 100 mL Teflon-lined stainless autoclave and placed in an oven (140 °C) for 12 h. After that we naturally cooled the solution to room temperature, centrifuged, and washed white precipitates with deionized water and ethanol repeatedly. The powder samples were fully dried in an oven (90 °C). To obtain Sm_2O_3 nanoroll sticks, we calcinated the $Sm(OH)_3$ nanoroll sticks at 450 °C for 4 h. The morphology of the samples was examined by scanning electron microscopy (SEM, Hitachi SE-4800). For the Sm_2O_3 nanoroll sticks, high resolution transmission electron microscopy (HRTEM) images were obtained using a Tecnai G2 F20 S-TWIN at an acceleration voltage of 200 kV. X-ray diffraction (XRD) patterns were recorded using a PANalytical X'Pert Pro MPD diffractometer with Cu Kα radiation. For the powder samples, diffuse reflectance UV–Vis–NIR absorption spectra were obtained using a Cary5000 spectrophotometer. Raman spectra were taken using a Bruker Senterra Raman spectrometer at a laser excitation wavelength of 532 nm. FT-IR spectra were obtained using a Thermo Scientific Nicolet iS10 spectrometer with ATR (attenuated total reflectance) mode.

Results and discussion

Figure 1 shows the SEM images of as-prepared and post-annealed (at 450 °C) Sm(III) powder samples. The as-prepared sample showed stick morphology with widths of 300–350 nm and lengths of 4–5 μm. The edges of the sticks showed open structure, indicating a tube-like morphology. For the thermal-annealed sample, the morphology was not significantly changed, however the sticks became significantly skinnier with widths of 200–250 nm. The shrinkage is due to a thermal dehydration effect. The color of the sample was white and unchanged after thermal annealing at 450 °C.

The XRD patterns of the as-prepared and 450 °C-annealed samples were obtained and are displayed in Fig. 2. The XRD patterns of the as-prepared sample matched well with those of the hexagonal phase (space group P63/m) $Sm(OH)_3$ (JCPDS 01-083-2036) well. Three major peaks were found at $2\theta = 16.0°$, 28.0°, and 29.2°, assigned to the (100), (110), and (101) planes, respectively. Other crystal planes were also assigned to the corresponding XRD peaks in Fig. 2. For the formation of $Sm(OH)_3$, a following reaction is proposed: $2Sm^{3+}$ (aq) + $3SO_4^{2-}$ (aq) + $6OH^-$ (aq) + $6NH_4^+$ (aq) → $2Sm(OH)_3$ (s) + $3SO_4^{2-}$ (aq) + $6NH_4^+$

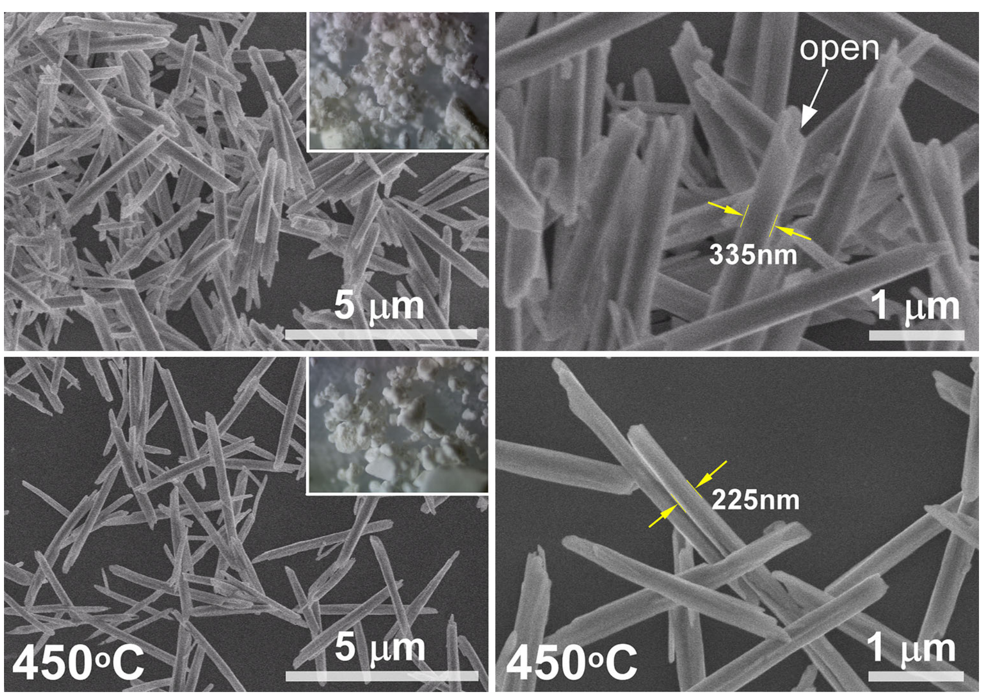

Fig. 1 SEM images of as-prepared (*top*) and 450 °C-annealed (*bottom*) samples. *Insets* show optical microscope images of the corresponding samples

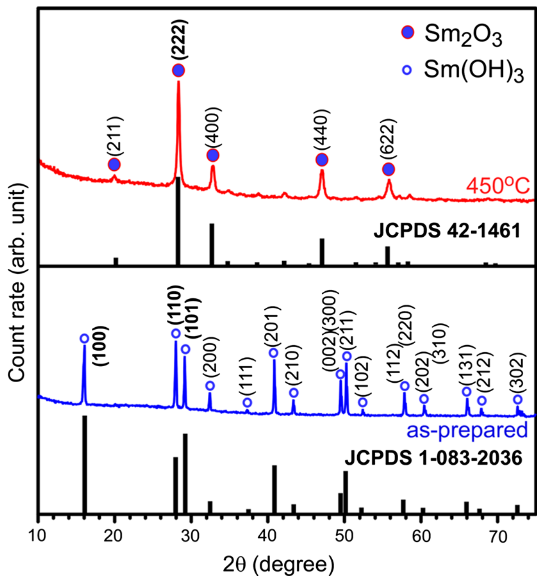

Fig. 2 Powder X-ray diffraction patterns of as-prepared (*bottom*) and 450 °C-annealed (*top*) samples. The reference XRD patterns are also shown below the corresponding XRD patterns

(aq) [11]. At lower concentrations of ammonia, SO_4^{2-} ions may also be participated to form Sm(OH)(SO_4). To confirm this scenario, we also synthesized with a smaller amount of ammonia (1.0 mL), and obtained a plate morphology showing a different crystal structure. This indicates that the plates consist of different Sm complexes which are under investigation. When we added 1.5 mL of ammonia we obtained mixed morphologies; SEM and XRD confirmed not shown here. Base on this, we conclude that the amount of ammonia plays a major role in determining the morphology. At a higher reaction temperature of 210 °C (not shown here), we found that the plates became thicker and the roll sticks became more like rods. For the thermal-annealed sample, the XRD patterns were drastically different from those of as-prepared sample. The patterns were in good match with those of cubic (space group Ia-3) phase Sm_2O_3 (JCPDS 42-1461). A major peak was found at $2\theta = 28.3°$ and assigned to the (222) plane. Other minor peaks at $2\theta = 19.9°$, 32.8°, 47.0°, and 55.8° were assigned to the (211), (400), (440), and (622) planes, respectively.

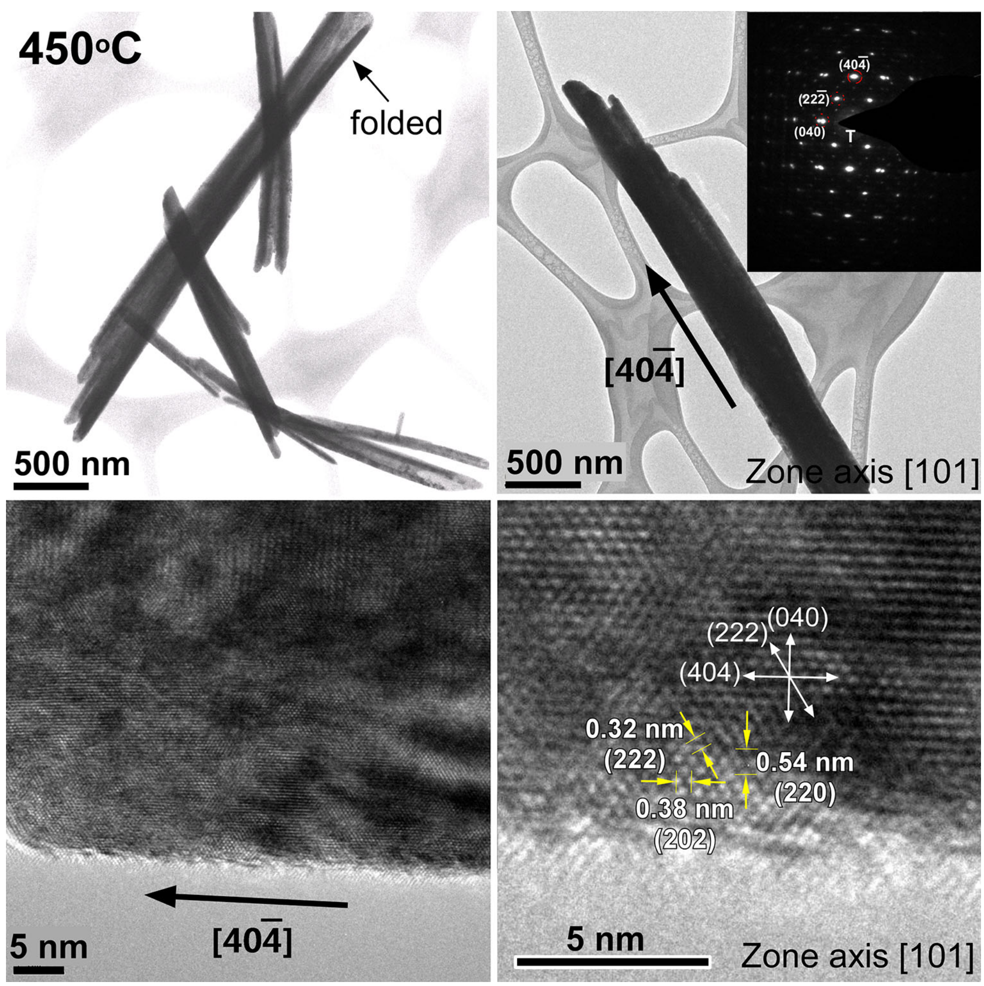

Fig. 3 TEM and HRTEM images, and SAED patterns (*inset*) of Sm_2O_3 nanoroll sticks

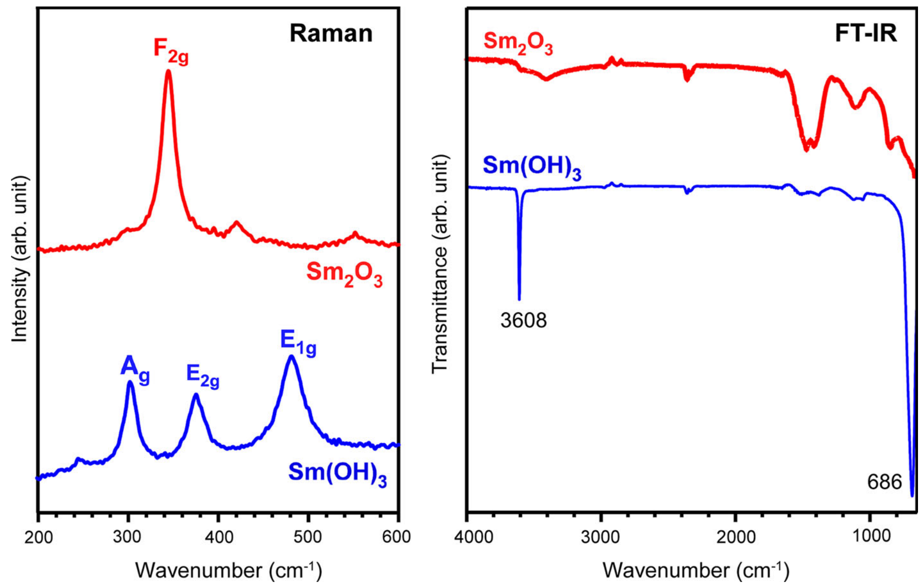

Fig. 4 Raman (*left*) and FT-IR (*right*) spectra of $Sm(OH)_3$ and Sm_2O_3 nanoroll sticks

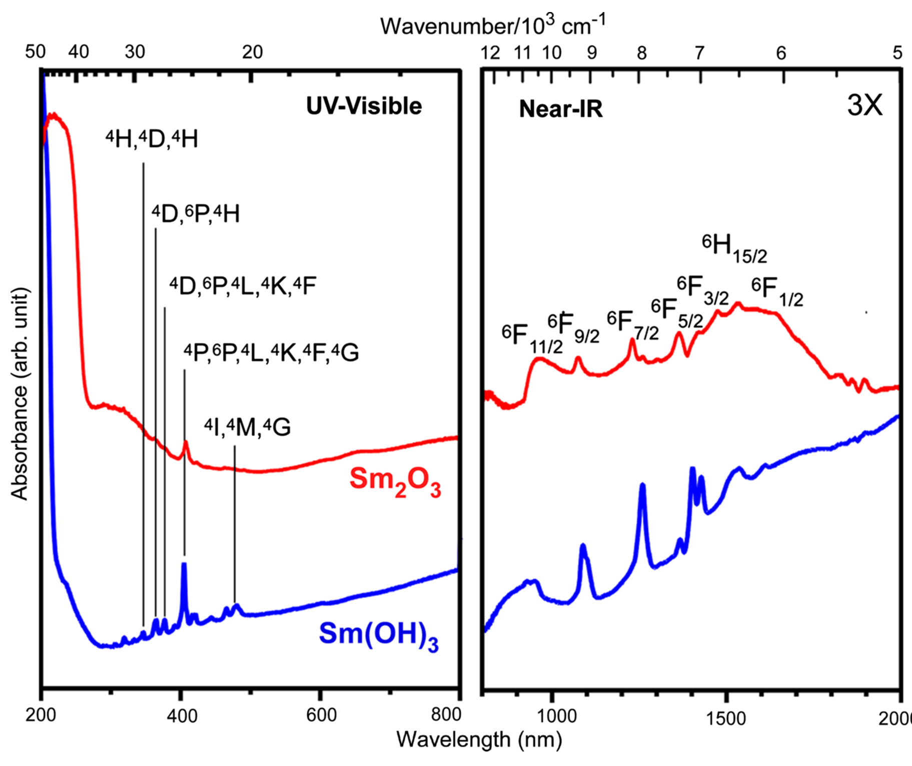

Fig. 5 UV–Visible reflectance absorption spectra of $Sm(OH)_3$ and Sm_2O_3 roll-sticks The spectral region in 900–2000 nm was 3× amplified for clear peak identification

Figure 3 displays the TEM and HRTEM images, and the selected area electron diffraction (SAED) patterns of Sm_2O_3 nanoroll sticks. As discussed above in Fig. 1, the TEM image clearly showed that a long roll sheet was folded to form a roll stick structure [22]. The SAED patterns along the [101] zone axis showed highly single crystalline nature of the nanoroll stick. The SAED pattern indicates that the crystal growth preferentially occurs along [40-4]. The HRTEM images showed clear lattice fringes. The distances between the planes were measured to be 0.32, 0.38, and 0.54 nm, which correspond the (222), (202), and (220) planes of cubic phase Sm_2O_3. On the basis of the results discussed above, we proposed the following growth mechanism. The nanoroll sticks may be formed by the following anisotropic growth and folding mechanism. $Sm(OH)(SO_4)$ seed with sheet morphology is initially formed, gradually transformed to $Sm(OH)_3$ and then the sheets anisotropically grow into longer sheets. Due to different growth directions, rates, and strains upon forming from $Sm(OH)(SO_4)$ to $Sm(OH)_3$ the sheets consequently

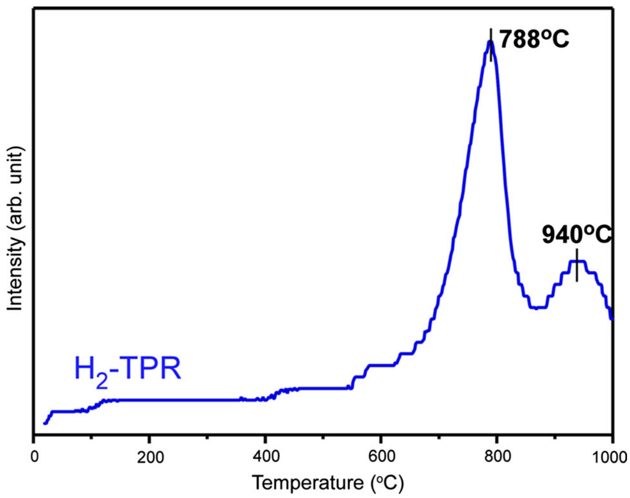

Fig. 6 Hydrogen temperature-programmed reduction (TPR) profile of Sm_2O_3 nanorods

roll up to form tubes (or roll stick-like structures at a lower temperature of 140 °C) or rods (at a high temperature of 210 °C).

The nanoroll sticks could also be synthesized for other rare earth compounds by a facial hydrothermal method by controlling the amount of ammonia and a reaction temperature. Sohn et al. have also synthesized other rare earth compounds including Dy(III) and Tb(III) and found similar morphological changes [27, 28]. Sheet morphology has commonly been obtained and converted to tube or rod morphology.

Figure 4 shows Raman and FT-IR spectra of $Sm(OH)_3$ and Sm_2O_3 nanoroll sticks. For $Sm(OH)_3$ nanoroll sticks, three major Raman peaks were observed at 302.0, 375.4, and 481.0 cm^{-1}, which could be assigned to A_g translatory, E_{2g} translatory, and E_{1g} libration modes, respectively [16]. For $Sm(OH)_3$ with a hexagonal crystal phase (P63/m), the vibrational mode representations are $4A_g + 3B_g + 2E_{1g} + 5E_{2g} + 2A_u + 4B_u + 4E_{1u} + 2E_{2u}$, where $4A_g$, $2E_{1g}$ and $5E_{2g}$ are Raman active. For Sm_2O_3 with a cubic phase, 22 Raman active modes of $4A_g$, $4E_g$, and $14F_g$ are expected [29, 30]. The strong Raman peak at 344.7 cm^{-1} was assigned to the combination of A_g and F_g modes [29, 30]. For the FT-IR spectrum of $Sm(OH)_3$, a very sharp IR peak was observed at 3608.0 cm^{-1} and attributed to the O–H stretching vibration [16, 31, 32]. The peak at 685.6 cm^{-1} was due to bending vibration of Sm–O–H [16]. For Sm_2O_3, a broad peak at 3400 cm^{-1} was due to H_2O (or hydrated) adsorbed on the oxide surface. The peaks at 1412 and 1473 cm^{-1} were commonly observed and attributed to symmetric and asymmetric stretching of COO^-, respectively [15].

Figure 5 displays the diffuse reflectance UV–Vis–NIR absorption spectra of $Sm(OH)_3$ and Sm_2O_3 nanoroll stick

Table 1 Summary of literature reported for $Sm(OH)_3$ and Sm_2O_3

Experimental condition and method	Morphology and size	Experimental data shown
$Sm(NO_3)_3 \cdot 6H_2O$, NH_4OH, precipitation method [11]	$Sm(OH)_3$ and Sm_2O_3 nanorods 30–150 nm wide and 150–350 nm long	XRD, HRTEM, TG, BET
$Sm(NO_3)_3$ sol., a surfactant, triethylamine, precipitation and heating (600 and 900 °C) [12]	Sm_2O_3 nanoparticles, nanorods, nanoplates	SEM, XRD, PL, magnetic susceptibility
$Sm(NO_3)_3 \cdot 6H_2O$, NaOH in supercritical water, hydrothermal method [14]	Sm_2O_3 nanoparticles, 50–80 nm	XRD, TEM, BET
$Sm(NO_3)_3$ sol., toluene, a capping agent, t-butylamine, hydrothermal method (120–200 °C) [15]	Sm_2O_3 nanoparticles and nanorods, 7–25 nm wide and 100–160 nm long	XRD, TEM, XPS, FT-IR, TG/DTA, BET
$SmCl_3 \cdot 6H_2O$, a surfactant (CTAB), NH_4OH, precipitation method [16]	$Sm(OH)_3$ nanorods, 15–90 nm wide and 120–500 nm long	SEM, XRD, HRTEM, FT-IR, Raman UV–Vis absorption,
$Sm(acac)_3$ in benzyl alcohol at 200 °C, Sol–gel method and calcination at 500 °C [18]	ultrathin Sm_2O_3 nanodisks	SEM, XRD, HRTEM
$Sm(NO_3)_3 \cdot 6H_2O$, sucrose, citric acid, PMMA microsphere template in methanol [19]	Sm_2O_3 mesoporous walls	SEM, XRD, HRTEM, UV–Vis–NIR absorption, Raman, FT-IR, PL,TG/DSC, BET
Sm(III) acetate + oleylamine + a long-chain carboxylic acid thermal decomposition [20]	Sm_2O_3 nanorods, 1.2 nm wide and 4–5 nm long	HRTEM, XRD
Sm(III) acetate + oleylamine + oleic acid microwave [21]	Sm_2O_3 nanowires, nanoplates, single unit cell size (1.1 nm × 2.2 nm)	HRTEM, XRD
Sm(III) nitrate sol, KOH (180 °C and 12 h), hydrothermal method [22]	$Sm(OH)_3$ nanowires, 20–30 nm wide and 2–5 μm long	XRD, HRTEM
$Sm_2(SO_4)_3 \cdot 8H_2O$, NH_4OH in water (140 °C, 12 h), hydrothermal method (*this study*)	$Sm(OH)_3$ and Sm_2O_3 nanoroll sticks, ~300 nm wide and ~5 μm long	SEM, XRD, HRTEM, UV–Vis absorption, FT-IR, TG/DSC, TPR

powder samples. The Y-axis was converted from the reflectance data using the Kubelka–Munk method. Although the intensities were different before and after thermal annealing all the UV–Vis–NIR absorption peaks were in good match with the electronic transitions of Sm(III) [19, 33].The absorption spectra between 900 and 2000 nm correspond to the f–f transitions from the ground state of $^6H_{5/2}$ to $^6F_{1/2,3/2,5/2,7/2,9/2,11/2}$ and $^6H_{15/2}$ energy levels as assigned on the corresponding peaks [33]. The absorption peaks found between 300 and 500 nm were assigned on the corresponding peaks. The broad absorption below 300 nm was possibly due to the O^{2-}–Sm^{3+} charge-transfer [19]. Zhang et al. reported very similar UV–Vis absorption profiles between 200 and 600 nm for Sm_2O_3 mesoporous walls [19].

We examined surface activity of Sm_2O_3 nanoroll sticks by recording temperature-programmed hydrogen reduction profiles as shown in Fig. 6. The hydrogen consumption was gradually increased from 400 °C. The gradual increase was commonly attributed to the reduction of surface oxide [34]. Above 700 °C, two broad and strong reduction peaks appeared at 788 and 940 °C. The former (major) peak at 788 °C was plausibly due to reduction process of Sm_2O_3 → SmO and the latter (minor) peak to SmO → Sm.

To show the originality of the nanoroll sticks, we summarized the previously reported results for $Sm(OH)_3$ and Sm_2O_3 in Table 1. Various morphologies have previously been reported using diverse synthetic methods. However, nanoroll stick morphology has never been reported so far.

Conclusion

Hexagonal phase $Sm(OH)_3$ nanoroll sticks were synthesized by a hydrothermal method for the first time. Highly single crystalline cubic phase Sm_2O_3 nanoroll sticks were obtained by post-thermal annealing at 450 °C. Growth direction of the oxide was found to be [40-4]. The crystal phases were confirmed by XRD, HRTEM, Raman, and FT-IR spectra. The UV–Vis–NIR absorption peaks of $Sm(OH)_3$ and Sm_2O_3 clearly showed the electronic transitions of Sm(III). The TPR peaks at 788 and 940 °C were attributed to reductions of Sm_2O_3 and SmO, respectively.

Acknowledgements This work was supported by the 2014 Yeungnam University research Grant.

References

1. Wu MH, Cheng CH, Lai CS, Pan TM (2009) Structural properties and sensing performance of high-k Sm_2O_3 membrane-based electrolyte–insulator–semiconductor for pH and urea detection. Sens Actuators B 138:221–227
2. Michel CR, Martinez-Preciado AH, Parra R, Aldao CM, Ponce MA (2014) Novel CO_2 and CO gas sensor based on nanostructured Sm_2O_3 hollow microspheres. Sens Actuators. doi:10.1016/j.snb.2014.06.038
3. Chin WC, Cheong KY, Hassan Z (2010) Sm_2O_3 gate dielectric on Si substrate. Mater Sci Semicond Proc 13:303–314
4. Huang SY, Chang TC, Chen MC, Chen SC, Lo HP, Huang HC, Gan DS, Sze SM, Tsai MJ (2011) Resistive switching characteristics of Sm_2O_3 thin films for nonvolatile memory applications. Solid-State Electron 63:189–191
5. Wang JC, Lu TF, Shih HY, Yang CM, Lai CS, Kao CH, Pan TM (2011) Reference electrode–insulator–nitride–oxide–semiconductor structure with Sm_2O_3 sensing membrane for pH-sensor application. Japan J Appl Phys 50:04DL09
6. Gao J, Zhao J, Yang W, Tian J, Guan F, Ma Y, Hou J, Kang J, Wang Y (2002) Preparation of samarium oxide nanoparticles and its catalytic activity on the esterification. Mater Chem Phys 77:65–69
7. Elkins TW, Hagelin-Weaver HE (2013) Oxidative coupling of methane over unsupported and alumina-supported samaria catalysts. Appl Catal A 454:100–114
8. Elkins TW, Neumann B, Baumer M, Hagelin-Weaver HE (2014) Effects of Li doping on MgO-supported Sm_2O_3 and TbO_x catalysts in the oxidative coupling of methane. ACS Catal 4:1972–1990
9. Liu S, Cai Y, Cai X, Li H, Zhang F, Mu Q, Liu Y, Wang Y (2013) Catalytic photodegradation of Congo red in aqueous solution by $Ln(OH)_3$ (Ln = Nd, Sm, Eu, Gd, Tb, and Dy) nanorods. Appl Catal A 453:45–53
10. Wang Y, Liu S, Cai Y, Deng S, Han B, Han R, Li Q, Wang Y (2014) $La(OH)_3$:Ln^{3+} (Ln^{3+} = Sm, Er, Gd, Dy, and Eu) nanorods synthesized by a facile hydrothermal method and their enhanced photocatalytic degradation of Congo red in the aqueous solution. Ceram Int 40:5091–5095
11. Xin Y, Wang Z, Qi Y, Zhang Z, Zhang S (2010) Synthesis of rare earth (Pr, Nd, Sm, Eu and Gd) hydroxide and oxide nanorods (nanobundles) by a widely applicable precipitation route. J Alloy Compd 507:105–111
12. Ghosh P, Kundu S, Kar A, Ramanujachary KV, Lofland S, Patra A (2010) Synthesis and characterization of different shaped Sm_2O_3 nanocrystals. J Phys D Appl Phys 43:4054011/1-7
13. Wang P, Bai B, Huang L, Hu S, Zhuang J, Wang X (2011) General synthesis and characterization of a family of layered lanthanide (Pr, Nd, Sm, Eu, and Gd) hydroxide nanowires. Nanoscale 3:2529–2535
14. Nejad SJ, Golzary A (2011) Experimental design for the optimization of hydrothermal synthesis of samarium oxide (Sm_2O_3) nanoparticles under supercritical water condition. Int J Chem Eng Appl 2:243–247
15. Nguyen TD, Mrabet D, Do TO (2008) Controlled self-assembly of Sm_2O_3 nanoparticles into nanorods: simple and large scale synthesis using bulk Sm_2O_3 powders. J Phys Chem C 112:15226–15235
16. Mu Q, Wang Y (2011) A simple method to prepare $Ln(OH)_3$ (Ln = La, Sm, Tb, Eu, and Gd) nanorods using CTAB micelle solution and their room temperature photoluminescence properties. J Alloy Compd 509:2060–2065
17. Xia T, Wang J, Lin N, Huo L, Zhao H, Mountrichas G (2010) Template-free synthesis, growth mechanism and photoluminescent properties of $Ln(OH)_3$ and Ln_2O_3 nanorods (Ln: lanthanide ion). J Alloy Compd 507:245–252
18. Xiao H, Li P, Jia F, Zhang L (2009) General nonaqueous sol-gel synthesis of nanostructured Sm_2O_3, $Gd_2O_3$3, Dy_2O_3, and Dy_2O_3:Eu^{3+} Phosphor. J Phys Chem C 113:21034–21041
19. Zhang H, Dai H, Liu Y, Deng J, Zhang L, Ji K (2011) Surfactant-mediated PMMA-templating fabrication and characterization of

three-dimensionally ordered macroporous Eu_2O_3 and Sm_2O_3 with mesoporous walls. Mater Chem Phys 129:586–593
20. Panda AB, Glaspell G, El-Shall MS (2007) Microwave synthesis and optical properties of uniform nanorods and nanoplates of rare earth oxides. J Phys Chem C 111:1861–1864
21. Yu T, Joo J, Park YI, Hyeon T (2006) Single unit cell thick samaria nanowires and nanoplates. J Am Chem Soc 128:1786–1787
22. Wang X, Yadong L (2002) Synthesis and characterization of lanthanide hydroxide single-crystal nanowires. Angew Chem Int Ed 41:4790–4793
23. Xu Z, Li C, Yang P, Hou Z, Zhang C, Lin J (2009) Uniform $Ln(OH)_3$ and Ln_2O_3 (Ln = Eu, Sm) submicrospindles: facile synthesis and characterization. Cryst Growth Des 9:4127–4135
24. Liu T, Zhang Y, Shao H, Li X (2003) Synthesis and characteristics of Sm_2O_3 and Nd_2O_3 nanoparticles. Langmuir 19:7569–7572
25. Panda PK (2013) Preparation and characterization of samaria nanofibers by electrospinning. Ceram Inter 39:4523–4527
26. Liu P, Wang Y, Wang X, Yang C, Yi Y (2012) Polypyrrole-coated samarium oxide nanobelts: fabrication, characterization, and application in supercapacitors. J Nanopart Res 14:1232/1-11
27. Kang JG, Gwag JS, Sohn Y (2014) Synthesis and characterization of $Dy(OH)_3$ and Dy_2O_3 nanorods and nanosheets. Ceram Int. doi:10.1016/j.ceramint.2014.11.085
28. Sohn Y (2014) Structural and spectroscopic characteristics of terbium hydroxide/oxide nanorods and plates. Ceram Int 40:13803–13811
29. Jiang S, Liu J, Lin C, Li X, Li Y (2013) High-pressure x-ray diffraction and Raman spectroscopy of phase transitions in Sm_2O_3. J Appl Phys 113:113502/1-6
30. Dilawar N, Mehrotra S, Varandani D, Kumaraswamy BV, Haldar SK, Bandyopadhyay AK (2008) A Raman spectroscopic study of C-type rare earth sesquioxides. Mater Character 59:462–467
31. Kang JG, Min BK, Sohn Y (2015) Physicochemical properties of praseodymium hydroxide and oxide nanorods. J Alloy Compd 619:165–171
32. Kang JG, Jung Y, Min BK, Sohn Y (2014) Full characterization of $Eu(OH)_3$ and Eu_2O_3 nanorods. Appl Surf Sci 314:158–165
33. Xu S, Zhu Y, Xu W, Dong B, Bai X, Xu L, Miao C, Song H (2012) Observation of ultrabroad infrared emission bands in Er_2O_3, Pr_2O_3, Nd_2O_3, and Sm_2O_3 polycrystals. Appl Phys Exp 5:102701/1-3
34. Lee SW, Park SK, Min BK, Kang JG, Sohn Y (2014) Structural/spectroscopic analyses and $H_2/O_2/CO$ responses of thulium(III) oxide nanosquare sheets. Appl Surf Sci 307:736–743